Signals of the liquid–gas phase transition in the fragmentation of hot nuclei: Finite–size scaling

Article *in* Nuclear Physics A · March 1991

DOI: 10.1016/0375-9474(91)90029-6

2 authors, including:

Henry Giacaman
Birzeit University
29 PUBLICATIONS **788** CITATIONS

Nuclear Physics **A524** (1991) 321-343
North-Holland

SIGNALS OF THE LIQUID–GAS PHASE TRANSITION IN THE FRAGMENTATION OF HOT NUCLEI: FINITE-SIZE SCALING

H.R. JAQAMAN[1,2,*] and D.H.E. GROSS[1,3]

[1] *Hahn-Meitner-Institut, Bereich Kern-und Strahlenphysik, W-1000 Berlin 39, Germany*
[2] *Physics Department, Birzeit University, Birzeit, West Bank*
[3] *Fachbereich Physik der Freien Universität, Berlin, Germany*

Received 10 August 1990
(Revised 20 September 1990)

Abstract: The distributions of fragments produced in events involving the multifragmentation of hot nuclei are compared with the cluster distributions predicted by a bond percolation model on a finite lattice. The nuclear events are generated by a microcanonical Metropolis sampling method. This comparison makes it possible within the model to separate the events due to the nuclear liquid-gas phase transition from the "hot fission" events. The latter events correspond to a phenomenon that is peculiar to the nuclear case and that reflects the role of the long-range Coulomb force. Finite-size scaling methods are used to analyze the percolation and nuclear liquid-gas phase transitions and to determine the appropriate critical exponents. The influence of the Coulomb force on the critical behaviour of the nuclear liquid-gas phase transition is discussed.

1. Introduction

The possibility of the occurrence of a liquid-gas transition in the fragmentation of hot nuclei has been the subject of several investigations [1,4]). Theoretical studies [5-11]) indicate that infinite chargeless nuclear matter has an equation of state very similar to that for an ordinary fluid or Van der Waals gas. Such a fluid is characterized by the existence of a liquid to gas phase transition with a critical temperature T_c. For temperatures T above T_c only a single gaseous phase exists consisting of single particles and small droplets or clusters. In the nuclear case the single particles would be the free nucleons. Below T_c two phases can exist: a liquid state (equivalent to an infinite cluster or condensate) coexists with its vapor. It has thus been argued that if a nucleus (which is the finite nuclear equivalent of the infinite liquid condensate) is heated to temperatures $\approx T_c$, it can undergo a phase transition to the gaseous phase. This approach has been put forward as an explanation for the fragment distributions observed in inclusive high-energy proton-nucleus reactions [12]) as well as in medium-energy heavy-ion collisions [13]).

However, there is a much more fundamental reason for studying the possible liquid-gas transition in *nuclei*. The usual interest in the study of phase transitions comes from the fact that, at the critical point, correlations in systems with short-range

* Alexander von Humboldt fellow.

interactions are much longer than the range of the forces. Consequently details of the interaction are unimportant and the phase transitions are ruled by geometrical properties of the system. Various systems fall into few different classes concerning their critical behaviour.

Nuclei are distinct from normal macroscopic systems by the fact that they are finite and subjected to the long-range Coulomb force. These two factors lead to a substantial modification of the properties of hot nuclei and the associated phase transitions [14-18]). Near T_c the correlation length is not the only relevant length in the system and the critical behaviour will be strongly modified. In particular a new phenomenon, which we will refer to as hot fission, appears. This reflects the massive population of a new region in phase space.

Another system in which a similar long-range repulsive force may modify the critical behaviour is a fast rotating star. Here the abundent occurrence of double stars might be related to this opening up of the additional phase space connected with fission. Although this stellar problem is interesting and worthy of a serious investigation we nevertheless do not pursue it any further beyond noting the possible analogy. The present work is restricted to nuclei which, anyway, are much more easily accessible experimentally.

These effects of the long-range force can of course be studied only in finite systems. The properties of a phase transition are, however, modified by finite size. Strictly speaking, a phase transition is well defined only for an infinite system in that the singularities and discontinuities that are associated with such a transition can only be observed in the thermodynamic limit. If the system has a finite size then this finite size affects the properties of the transition: the singularities become finite and the discontinuities are replaced by smooth jumps [19]).

A promising method to overcome this inherent difficulty of the nuclear case has been suggested by Campi [20,21]). It consists of comparing the properties of the liquid-gas phase transition in the nuclear case with the properties of percolation on finite lattices of a similar size. As the infinite system exists for the percolation problem, a comparison between systems of comparable size in the two cases is expected to deal, at least partially, with the finite-size problem.

The effects of the finite size on the properties of percolation or thermal phase transitions are rather well studied and are described by various finite-size scaling ansatzes and hypotheses [22,23]). In addition, an interesting feature of percolation is that it is a very simple model of a phase transition depending only on local geometry so that any significant deviations of the nuclear case from the properties predicted by percolation may be attributed to the role of the long-range Coulomb force.

In an earlier work [4]), hereafter referred to as (I), the fragmentation of hot nuclei was studied within the microcanonical metropolis sampling method of Gross *et al.* [24,25]) and a comparison was carried out between nuclear fragmentation and the cluster distributions obtained within the bond percolation model along the lines suggested by Campi [20,21]). A large number of events were generated in each model

(about 2 million events for percolation and 10 million for nuclear fragmentation) and these events were analyzed by calculating the conditional moments of the fragment (or cluster) size distribution for each event separately and then studying the distributions of these moments.

In particular by studying the correlation between the largest fragment in each event and the second moment of the distribution of the remaining fragments it was found that there were similarities and differences between the predictions of the two models. The correlation in the percolation model showed the typical features that reflect the occurrence of a phase transition (see fig. 1 below) in that it consisted of two branches: an upper branch with a negative slope that corresponds in the average to events with a bond probability p greater than a critical bond probability p_c and a lower branch with a positive slope that corresponds in the average to events with $p < p_c$. The two branches meet at the critical point of the percolation phase transition.

The correlation found for the nuclear case had also such a two-branch feature which is believed to reflect the occurrence of the liquid-gas phase transition in nuclear matter. In this case, in the average, the upper branch corresponds to events with temperature T less than the critical temperature T_c and the lower branch corresponds to events with $T > T_c$.

However, the nuclear case was found to have additionally a concentration of hot fission events that are rather well-separated from these two branches. These events are marked by large values for P and S_2 and they reflect the opening-up of additional phase space caused by the interplay between the surface energy and the long-range Coulomb force that is peculiar to the nuclear case. It must be stressed that these hot fission events are quite different from the customary "cold fission" in nuclear physics. For one thing, the energy deposited in the hot nucleus that produces such events is several hundred MeV. In addition the two big fragments are produced in conjunction with a sizeable number of various-sized small fragments.

Therefore, in order to display the analogy between the liquid-gas phase transition in the nuclear case and the percolation phase transition, *it is important that the hot fission events are excluded from the nuclear results before any analysis is carried out.* It is however an open question whether this method of simply excluding the hot fission events is sufficient to get rid of the effects of the long-range Coulomb force. To study this question is one of the main issues of this paper.

The calculations carried out in (I) were limited in the nuclear case to the study of the fragment charge distributions of gold nuclei ($Z = 79$), and in the percolation case to bond percolation on a cubic lattice with 4^3 sites. In the present work the calculations are extended to include systems other than those in (I) both for the nuclear case and the percolation case. Finite-size scaling is employed to study the critical behaviour in both cases. Since the properties of the percolation phase transition are relatively well-understood, the present percolation calculations serve also to examine the reliability of the methods to be employed for the nuclear case.

This is important since the sizes of the systems involved in the present work are much smaller than those usually employed to study finite-size scaling.

In sect. 2 we summarize the scaling properties of phase transitions that are to be used in our analysis. In sect. 3 the results for the percolation case are presented. Sect. 4 contains the details and results of the nuclear calculation. We present our conclusions in sect. 5.

2. Scaling properties of critical phenomena

Critical phenomena, such as the behaviour of percolation and liquid-gas phase transitions near their respective critical points, are ususally analyzed in terms of scaling hypotheses [26-28]). These hypotheses depend on the observation that the properties of the phase transition in the critical regime are dominated by a single factor which is the correlation length. This is the distance over which two particles or sites are correlated. The correlation length becomes very large (i.e. of the order of the linear size of the system) near the critical point. For an infinite system it actually diverges as

$$\xi(\varepsilon) \approx |\varepsilon|^{-\nu}, \tag{1}$$

where ν is a critical exponent and ε is a variable characterizing the state of the system. In thermal phase transitions $\varepsilon = T - T_c$ is the deviation from the critical temperature while in percolation $\varepsilon = p_c - p$ is the deviation from the threshold probability p_c. This divergence leads to large fluctuations. In the case of a liquid-gas phase transition these fluctuations lead to the phenomenon of critical opalescence [28]).

The dominance of the correlation length implies close similarity between various phase transitions at the critical point as the detailed properties of the various systems become immaterial and the phase transitions are governed by common geometrical features.

As an example, near the critical point a cluster size distribution of the general form

$$n(s, \varepsilon) \approx s^{-\tau} f(\varepsilon s^{\sigma}) \tag{2}$$

is predicted where s is the size of the cluster and τ and σ are two critical exponents. The Fisher doplet formula [29]) is a special case of eq. (2). At the critical point $\varepsilon = 0$, $f(0) = 1$ and the cluster distribution follows a power law:

$$n(s, 0) \approx s^{-\tau}. \tag{3}$$

In fact it was the observation [12]) that the light fragment distribution measured in inclusive high-energy proton-induced reactions followed such a power law that triggered the proposal of the existence of a liquid-gas phase transition in finite nuclei.

Another example that will be of interest in the present work is the size of the largest cluster which we denote as P. In the nuclear case the size of a fragment can be its mass or its charge while for percolation we choose the size of a cluster to mean the number of sites belonging to the cluster, rather than the number of bonds

between the sites, in order to make the analogy with the nuclear case more evident. The size of the largest cluster is expected to scale with the linear size L of the system in the following way [26]):

$$P(L, \varepsilon) \approx L^D H(\varepsilon L^{1/\nu}) \tag{4}$$

where the critical exponent D is the so-called fractal dimension of the system. The value of D at the critical point can be related to the other exponents [26]):

$$D = 1/\nu\sigma . \tag{5}$$

At the critical point $H = 1$ so that the size P_c of the largest cluster at the critical point is given by

$$P_c \approx L^D \tag{6}$$

that is, it is proportional to the linear size of the system raised to the power D rather than d the euclidean dimension. Away from the critical point the fractal dimension can assume different values. For example for percolation $D = d$ for $p > p_c$ [ref. [26])].

For the fragments or clusters produced in each event we can calculate the various moments of the cluster size distribution where the k^{th} moment is defined as follows

$$M_k = \Sigma n(s) s^k , \tag{7}$$

where $n(s)$ is the multiplicity of the clusters of size s and the summation is over all the clusters produced in the given event except for the largest cluster P. In the thermodynamic limit, P corresponds to the infinite percolating cluster in the percolation case, and to the condensate in the case of a liquid-gas phase transition.

Assuming a cluster multiplicity of the form given by eq. 2 and replacing the summation by an integration we get [26,27]);

$$M_k \approx |\varepsilon|^{(\tau-1-k)/\sigma} . \tag{8}$$

Since the exponent τ satisfies $2 < \tau < 3$ the second and higher moments diverge at the critical point. In contrast the lower moments M_0 and M_1, which correspond respectively to the number of fragments and the total mass, do not diverge. In particular the second moment diverges as

$$M_2 \approx |\varepsilon|^{-\gamma} , \tag{9}$$

where $\gamma = (3 - \tau)/\sigma$. For the nondiverging lower moments care must be taken when replacing the sum by an integral. In particular for the first moment M_1, a careful analysis shows that there is an additional constant term (see e.g. ref. [26])). We follow the suggestion of Campi [20]) and normalize the higher moments of the cluster size distribution for a given event by dividing them by the first moment

$$S_k = M_k / M_1 . \tag{10}$$

Another result that is of interest involves the relative size P/L^3 of the largest cluster for $\varepsilon < 0$ i.e. the percolating cluster (for $p > p_c$) or the liquid-condensate (for $T < T_c$). With ε sufficiently small we have for $\varepsilon < 0$ [refs. [26,27])]:

$$P/L^3 \approx |\varepsilon|^{\beta} , \tag{11}$$

TABLE 1

The values of the critical exponents for the percolation and liquid-gas phase transitions in 3 dimensions. For each case only two exponents are independent; the remaining exponents can be obtained from them through the scaling relations. The value of the fractal dimension is calculated from the relation $D = 1/\nu\sigma$

Exponent	Percolation [a])	Liquid-gas [b])
β	0.44	0.328 ± 0.008
γ	1.76	1.239 ± 0.002
ν	0.88	0.632 ± 0.002
τ	2.20	2.209
σ	0.45	0.638
D	2.53	2.480

[a]) From ref. [30]). [b]) From ref. [31]).

where a new critical exponent β has been introduced (it being understood that the proper value of β for the phase transition is that corresponding to the limit $L \to \infty$). However, not all the critical exponents are independent of each other as they are related by various scaling relations (see e.g. refs. [26,28])). In table 1 the values of the various critical exponents of interest to the present work are listed for both percolation and liquid-gas phase transitions. These are obtained from refs. [30,31]).

For $\varepsilon > 0$ there is no percolating cluster or condensate but the size of the typical finite cluster is expected to be approximately given by [20]):

$$s(\varepsilon) \approx \varepsilon^{-(\beta+\gamma)} . \tag{12}$$

This result follows from the location of the maximum of $n(s, \varepsilon)$ in eq. (2).

3. Finite-size scaling and the percolation problem

We consider percolation on a cubic lattice of linear size L containing L^3 sites, for $L = 4$ to 10, where all the sites are occupied and bonds are assumed to exist between neighbouring sites with bond probability p. Sites that are connected together by such bonds are said to belong to the same cluster. It is well known that in such a model there exists a critical (or threshold) probability p_c such that for $p > p_c$ there is a large cluster that percolates throughout the lattice from end to end whereas for $p < p_c$ no such cluster exists and all the sites belong to small clusters (including isolated sites, i.e. singlets or clusters of size 1). As $L \to \infty$ the phase transition becomes sharper and sharper and p_c approaches a limiting value which for bond percolation on a cubic lattice is $p_c = 0.2492$ [ref. [26])].

For finite systems the threshold percolation probability is not so sharply defined but this is not very important for the present work because we will not use the probability p directly in our analysis. Rather we will sample percolation events over

a certain probability interval that includes the critical region. A similar situation arises in the nuclear case where the critical point is not well defined for a finite nucleus. Here we also resort to sampling events over a certain energy distribution (energy or temperature being the thermal equivalent of the proability p). Moreover, in the theoretically generated nuclear events we have an additional reason to sample events from an excitation energy distribution over some suitable energy range. This is because in the experimental nuclear situation the excitation energy deposited in the fragmenting nuclear system is not unique and we get events that are distributed over some energy range that presumably includes the interesting critical region.

Furthermore we sample percolation events over a rather narrow interval surrounding p_c because we are mainly interested in events that are close to criticality and that produce a relatively large number of intermediate size clusters. Events with $p \ll p_c$ produce mainly singlet clusters that correspond to the noninteresting total vaporization situation in the nuclear case. Events with $p \approx 1$ produce mainly a single cluster that spans almost all the lattice sites. This would correspond to the case in which the nucleus stays intact or evaporates a few nucleons which is also of little interest. Moreover, it is not sufficient to take a uniform probability distribution in an interval containing p_c, as this does not produce enough events close to p_c to achieve statistical convergnce. For $p \approx p_c$ statistical fluctuations are very large and in order to achieve a reliable accuracy we have used a probability distribution peaked at p_c of the form:

$$\Pi(p) = (p - p_1)(p_2 - p), \qquad p_1 < p < p_2 \tag{13}$$

with $p_1 = 0.08$, $p_2 = 0.42$ and $\Pi(p) = 0$ outside this range.

The results for the case $L = 5$ are shown in fig. 1 where we plot the logarithm of the largest cluster P in each event versus the logarithm of the second moment S_2 of the size distribution of the remaining clusters in the event. The total number of events contributing to the plot is one million. The two branches corresponding to $p < p_c$ (lower branch) and $p > p_c$ (upper branch) are clearly seen. It is also evident that the area where the two branches meet (i.e. the critical region) is very well populated in contrast to the case where a uniform probability distribution is used as was done in (I).

It is not however possible from such a plot to locate the critical region in a precise and unambiguous manner. In order to be able to do that we calculate $\bar{S}_2$ the average of S_2 over all events belonging to the same value of ln P. The results obtained by such averaging are presented by the dots shown in fig. 2 where we plot ln P versus ln $\overline{S_2}$ for various cubic lattices with linear dimension $L = 4$ to 10 sites. The curves drawn through the dots are just to guide the eye. The location of the maximum value of $\overline{S_2}$ is now defined as corresponding to the location of the critical point which is a standard way of determining the percolation threshold [32]).

The size of the largest fragment at the critical point P_c as determined by the above criterion is plotted in fig. 3 versus the linear size of the system in a log-log plot for

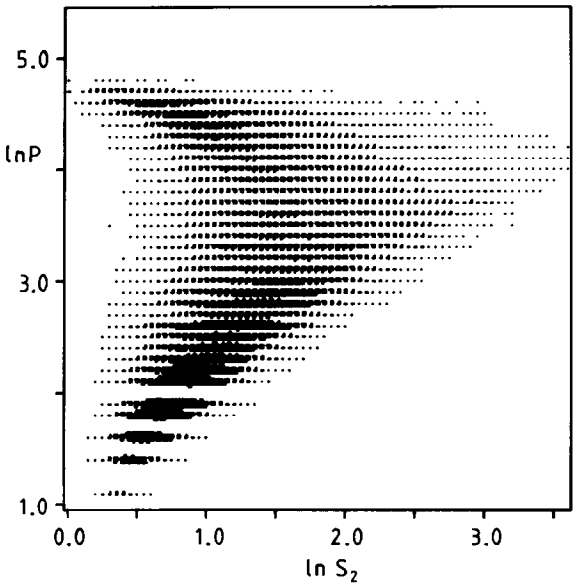

Fig. 1. The logarithm of the size of the largest fragment P produced per event as a function of the logarithm of the corresponding second moment S_2 for bond percolation on a simple cubic lattice of linear size $L = 5$ sites. The plot represents 10^6 such events and the size of the character plotted at each point is proportional to the number of events belonging to that point (which represents a bin in $\ln P \times \ln S_2$ space).

the various systems that are considered in fig. 2. The error bars in this figure reflect the size of the bins to which the values of $\ln P$ are assigned. The slope of the best straight line through the data points is then our estimate of the fractal dimension (see eq. (6)). This is found by a least-squares-method fit to be $D = 2.51 \pm 0.08$ which is in agreement with the result $D = 2.53$ for $L \to \infty$ quoted in table 1 indicating that the method utilized here is satisfactory.

The slopes of the lower branches of the curves in fig. 2 can also be calculated. From eqs. (9) and (12) this slope is expected [38]) to be $1 + \beta/\gamma$ which for percolation in 3 dimensions is equal to 1.25 when the values of the critical exponents given in table 1 are used. For comparison the slopes of the straight lines obtained by a lest-suares fit to the lower branches of the $L = 4$ to 10 curves in fig. 1 are found, in ascending order of L, to have the values 1.582 ± 0.036, 1.503 ± 0.029, 1.375 ± 0.017, 1.355 ± 0.021, 1.260 ± 0.007, 1.258 ± 0.014 and 1.242 ± 0.015. This indicates that these slopes rapidly approach the value expected in the thermodynamic limit. In calculating these slopes we have excluded the points near the bottom of the branch in the region where the curves in fig. 2 deviate noticeably from a straight line. These points correspond to events that are far removed from the critical region in which eqs. (9) and (12) are expected to apply. Furthermore, the lowest couple of points correspond to events with *low p* that come from the lower tail of the distribution in eq. (13)

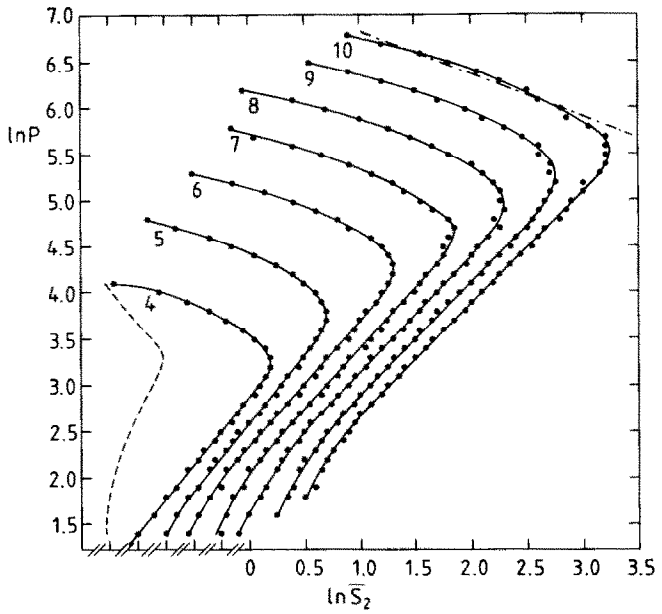

Fig. 2. The logarithm of the largest fragment size P as a function of the logarithm of the corresponding average second moment $\overline{S_2}$ for bond percolation on simple cubic lattices of linear sizes ranging from $L=4$ to 10 sites. The dots represent the actual calculation results and the curves drawn are just to guide the eye. The number next to each curve gives the value of the linear size L. Note that the ln $\overline{S_2}$ scale given corresponds to the $L=10$ curve. The other curves are successively shifted to the left with respect to each other by a distance of 0.25. The dashed curve and the dotted--dashed straight line are explained in the text.

and, hence, are not statistically reliable because of the low values of $\Pi(p)$ in this region.

Similarly, the upper branches in fig. 2 are also expected [38]) from eqs. (9) and (11) to be straight lines with a negative slope $-\beta/\gamma=-0.25$. In contrast to the lower branches, however, the upper branches are appreciably different from being straight lines indicating that one must go to larger systems in order to get straight lines whose slope can be measured with confidence. Nevertheless, we have measured the slope of the dotted-dashed straight line that is a reasonable fit to the $L=10$ upper branch data points and found that its slope is -0.45.

The dashed curve in fig. 2 is a plot of ln P versus ΔS_2 where ΔS_2 is the standard deviation in S_2 from its average value $\overline{S_2}$, for the $L=4$ case. Plots for other system sizes are similar and are not reproduced here. It is seen that ΔS_2 peaks at the same point (namely, the critical point) as $\overline{S_2}$ indicating that at this point the statistical fluctuations in S_2 become very large. This is related to the fact that the correlation length becomes very large near the critical point (see eq. (1)) which leads to large fluctuations. In other words these fluctuations are the percolation equivalent of critical opalescence seen in a liquid-gas phase transition. The fact that in fig. 2 both

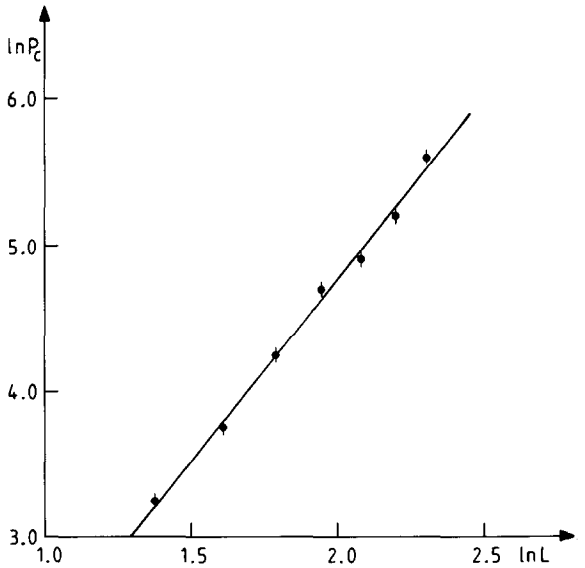

Fig. 3. The logarithm of the largest fragment size at the critical point P_c as a function of the logarithm of the corresponding linear size L for the various bond percolation systems of the previous figure.

the average S_2 and its standard deviation peak at the same value of P is further indication of the reliability of our method to determine the critical point.

One striking feature of fig. 2 is the general similarity between the shapes of the curves for the various systems. This is an indication that we should try to test a finite size scaling ansatz like eq. (4). By plotting P/L^D versus $\varepsilon L^{1/\nu}$, the curves for the various systems should collapse into one single curve for some appropriate values of D and ν. Eq. (4) cannot, however, be used directly for our present results because, as mentioned earlier, we do not have any knowledge of $\varepsilon = p_c - p$ for each event.

However, we can use the fact that S_2 depends on ε as in eq. (9) and try a finite-size scaling ansatz of the form

$$P(L, \varepsilon) \approx L^D J(S_2/L^\theta) . \tag{14}$$

The exponent θ can be related to the other exponents. By comparing eqs. (4) and (14), and making use of eq. (9) we get

$$\theta = \gamma/\nu \tag{15}$$

so that for percolation $\theta = 2.00$, where we have used the values of the critical exponents from table 1.

The results for various values of D and θ are shown in fig. 4. Ignoring, as discussed above, the unreliable bottom part of the lower branches, the best results are obtained

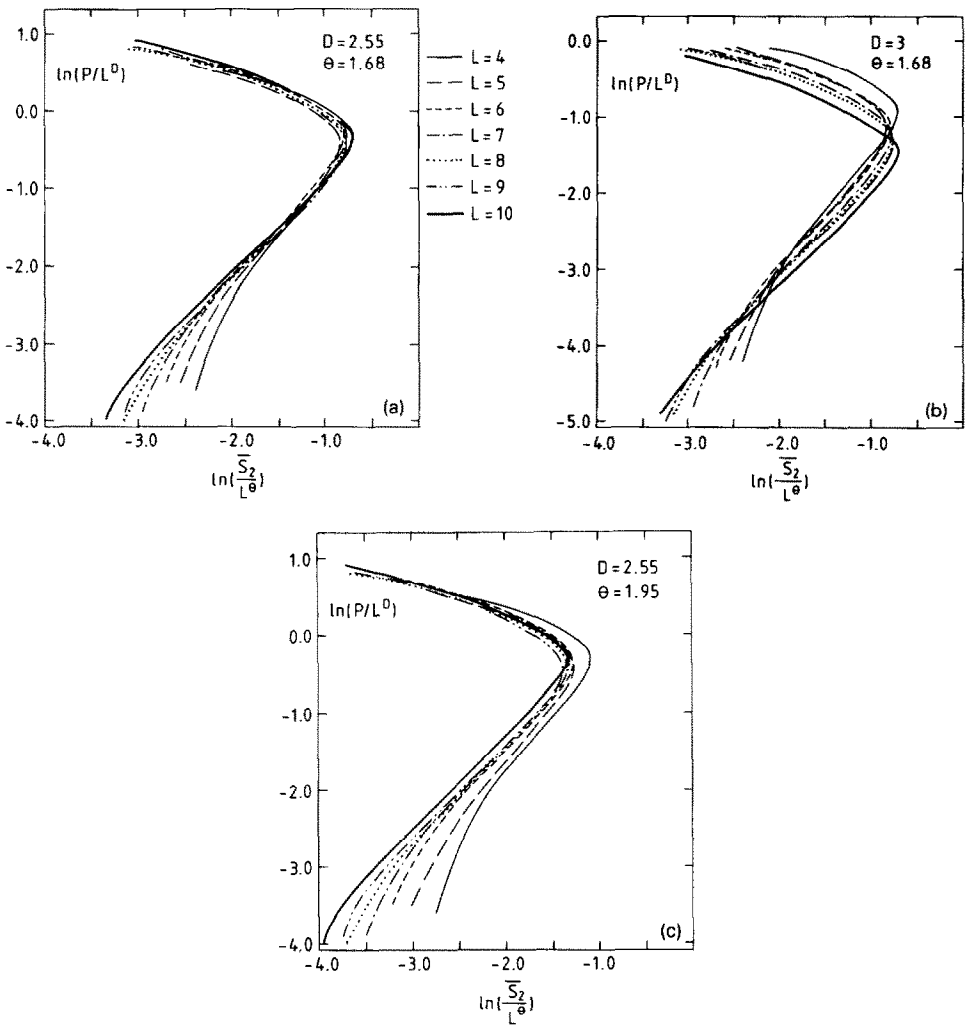

Fig. 4. Finite-size-scaling analysis of the $\ln P$ versus $\ln \overline{S_2}$ plots for the various percolation systems investigated. For clarity, we do not show the dots representing the actual results of the calculation, but we show smooth curves drawn through these dots similar to the curves drawn in fig. 2. (a): $D = 2.55$, $\theta = 1.68$; (b): $D = 3$; $\theta = 1.68$; (c): $D = 2.55$, $\theta = 1.95$.

for values of $D = 2.55$ and $\theta = 1.68$. The value for D is in excellent agreement with the values found in the literature (see table 1) and is consistent with the result obtained from fig. 3. It is evident that the fractal dimension must be different from the euclidean dimension since fig. 4b shows that for $D = d = 3$ the various curves do not overlap. The value of $\theta = 1.68$ obtained from fig. 4 is somewhat smaller than the expected value of $\theta = 2.00$ quoted above. This may reflect the fact that the systems considered are very small so that higher-order corrections to finite-size

scaling may be important. However, it was not attempted in the present work to go beyond the lowest-order scaling ansatz.

4. Finite-size scaling and nuclear fragmentation

We consider theoretical calculations of statistical decay of equilibrized hot nuclei in a microcanonical ensemble. In the method of microcanonical Metropolis Monte Carlo sampling we have a powerful mathematical method to simulate and predict the statistical decay of hot nuclei in a very realistic model. The statistical model of nuclear fragmentation [24,33,34]) allows a direct description of the most complicated thermodynamic phenomena like phase transitions and critical behaviour from first principles (direct calculation of the partition function). In the absence of experimental data with good statistics, the analysis of the theoretical results is the only possiblity at the moment.

In the present work we have carried out such calculations for 6 different nuclear systems. For each system the events are sampled over a certain excitation energy range that extends from an initial excitation energy $E_0^* = 200$ MeV (100 MeV for the 2 smallest systems) to some maximum excitation energy E_M^* that exceeds the total binding energy of the ground state of the system by about 50%. This energy range is divided into energy intervals of size 200 (or 100) MeV. The sampling is microcanonical in that a large number of events is sampled at a fixed total energy corresponding to the beginning of each of these intervals. However, in order to save computer time, we do not sample each event explicitly and completely. Rather we determine only the number and sizes of the fragments in an event, and integrate microcanonically over their momenta and all prompt neutrons [24,25]). Each sampled event is then analyzed separately and the relevant quantities, like the size of the largest fragment P and the second moment of the remaining fragments S_2, are calculated. The contributions of all the events are then put together to produce the final correlation between these quantities.

An important question that arises in this situation is what kind of excitation energy distribution must be used. In an experimental situation the excitation spectrum is determined by the dynamics of the reaction and the distribution at intermediate to high excitation energies is often found to fall off exponentially in a manner close to that predicted by the Glauber multiple scattering theory [35]). There is evidence, however, that at still higher energies the excitation energy distribution becomes uniform [36,37]). In fact, such an energy distribution (exponential + uniform) was used in our calculations reported in (I) to calculate the fragmentation of Gold nuclei in order to simulate the experimental situation as much as possible.

Such an excitation energy distribution is, however, not very suitable for our present purposes. Since it is peaked at low energies it tends to produce too many low-energy evaporation events that are not of interest to the present work. More important is that it tends to produce too many hot fission events that appear for

excitation energies up to about 800 MeV. Since, as explained earlier, these hot fission events are to be separated from the events to which the finite-size-scaling hypotheses are to be applied, it is important that as few as possible fission events are produced. This is in order not to make the final results very sensitive to the criteria by which these fission events are separated. Again this entails that the excitation energy spectrum should not be large at the energies at which fission contributes significantly. Finally a distribution peaked at low excitation energies does not produce enough events in the important critical region to achieve a satisfactory statistical accuracy. In order to overcome all these difficulties we use in the present work an excitation energy distribution peaked at the middle of the excitation interval:

$$\Pi(E^*) = [E^*(E^*_{\mathrm{M}} - E^*)]^2 . \tag{16}$$

The upper limit of the excitation spectrum E^*_{M} is typically taken about 1.5 times the binding energy of the ground state of the system.

Here it must be stressed that the results should not depend on the particular excitation energy distribution used provided that a large number of events is generated to achieve statistical convergence in the critical region in which we are interested. The use of various distributions merely changes the relative concentration of events along the various branches but not the shape of these branches or their slopes. The advantage of the distribution described by eq. (16) is that it allows adequate statistical reliability in the critical region in a reasonable amount of computer time.

Figs. 5 and 6 show nonaveraged plots of ln P versus ln S_2 for the cluster charge distributions of ^{197}Au and ^{232}Th. The Au results are produced from (I) where they were calculated with an energy distribution peaked at low energies while the Th results were calculated using the excitation energy distribution given by eq. (16) with E^* changing in steps of 200 MeV from an initial exitation $E^*_0 = 200$ MeV up to $E^*_{\mathrm{M}} = 2600$ MeV. Each figure is generated by about 10 million nuclear fragmentation events obtained by microcanonical Metropolis sampling. In both figures we see clearly the two branches corresponding to the liquid-gas phase transition and the separate concentration of hot fission events in the upper-right corner. This is in contrast to the percolation plot given in fig. 1 where the fission events are clearly absent. The critical region in the Th case is much better populated and hence more statistically reliable than in the Au case as a result of the energy distribution used (eq. (16)). The contrast between the two critical regions is actually more than it appears in the figures as the critical region in the Au plot was artificially enhanced by suppressing the intensity of the other parts. This was done in order to show the details of the region where the two branches meet, since the excitation spectrum used in (I) for the Au case produced too few events in the critical region.

In contrast to the Au plot, the Th plot has very few events with very large P (evaporation events) or very small P (vaporisation events) as a result of the energy distribution (eq. (16)) which was used for this purpose. This leaves the larger part

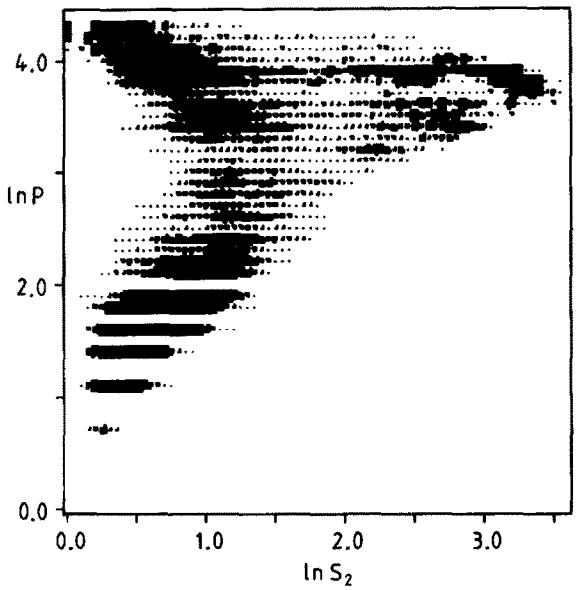

Fig. 5. The logarithm of the largest fragment charge $P(=Z_1)$ produced per event as function of the logarithm of the corresponding second moment S_2 for the microcanonical multifragmentation of hot ^{197}Au nuclei. The plot represents 10^7 such events and the size of the plotted characters has the same meaning as in fig. 1. However in order to enhance the details of the plot in the lightly populated critical region, the intensity maximum which occurs at the uppermost left point of the plot has been suppressed by a factor of 32.

of the events in the interesting critical region. The fission events that are to be removed from the Th calculation lie to the right of the thin continuous zig-zag line drawn in fig. 6, as explained below. If these events are excluded, then the remaining plot is similar to that obtained in percolation in its shape (see fig. 1) although it does have a richer topographical structure than its percolation equivalent. This structure reflects the more complicated nature of the nuclear problem in contrast to the extremely simple percolation problem which depends only on local geometrical properties.

Despite the fact that the energy distribution of eq. (16) was designed to reduce the number of hot fission events, we still have a large number of such events in the Th case (fig. 6). This reflects the fact that the fissility of such a heavy nucleus is large. An energy distribution peaked at lower energies, as in the experimental situation, would have produced many more fission events and would have made the problem of removing the fission events more difficult. This would mean, of course, that experimental data would be much more difficult to analyze than the theoretically generated events treated here. A large number of fission events must be removed before getting to the events involved in the liquid-gas phase transition.

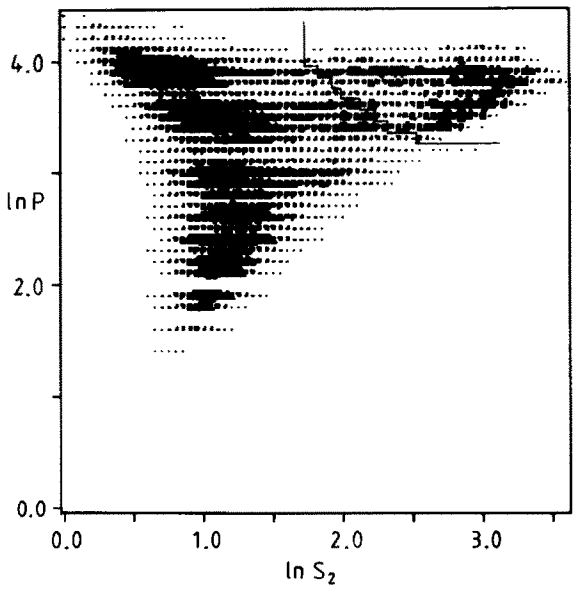

Fig. 6. The logarithm of the largest fragment charge $P(=Z_1)$ produced per event as a function of the logarithm of the corresponding second moment S_2 for the microcanonical multifragmentation of hot ^{232}Th nuclei. The plot represents 10^7 such events and the size of the plotted characters has the same meaning as in fig. 1.

The subtraction of the hot fission events is most easily carried out by considering the product Z_1Z_2 of the largest two fragment charges in each event. It was demonstrated in (I) that the hot fission events have the largest values of Z_1Z_2 and form a peak that is relatively well separated from the rest of the events. Fig. 7 shows a log-log plot of Z_1Z_2 versus S_2' for the case of ^{232}Th, where S_2' is the second moment of the fragment charge distribution (eq. (10)) with the largest two fragment charges Z_1 and Z_2 excluded. The events used to generate this figure are the same as those used to generate fig. 6. It is seen that the fission events are separated by a rather wide "valley" from the main peak containing the rest of the events and this provides a practical way to carry out the removal of the hot fission events. As demonstrated in (I), the percolation events populate only the main peak and do not produce an additional peak corresponding to the fission events in the nuclear case.

The removal of the fission events must, however, be done very carefully since their contribution to the average value $\overline{S_2}$ can be very large. Because of the large values of S_2 for such events, which is due to the fact that the square of Z_2 is very large, the removal of a relatively small number of fission events can appreciably modify the value of $\overline{S_2}$. This point is very important because of the width of the valley separating the fission events from the rest (see fig. 7) so that it is not apparent where the cut must be made. In order to effect the removal of the hot fission events

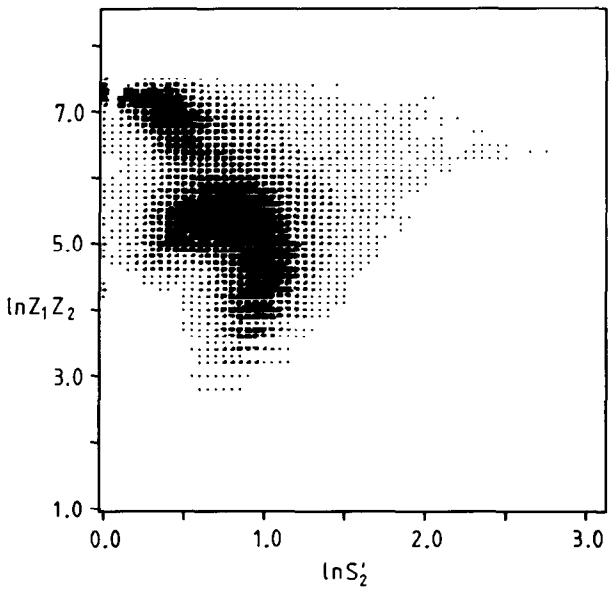

Fig. 7. The logarithm of the product of the largest two fragment charges Z_1Z_2 produced per event as a function of the logarithm of the corresponding second moment S_2' for the microcanonical multifragmentation of hot ^{232}Th nuclei. The plot represents the same events as in fig. 6. The size of the plotted characters has the same meaning as in fig. 1.

in a satisfactory manner we have employed additional criteria that must be satisfied. One such criterion is that the cut we make must also correspond to a naturally occurring "valley" in a plot of P versus S_2 like that of fig. 6. Another criterion is that the cut produce a smooth averaged plot of $\ln P$ versus $\ln \overline{S_2}$ similar to that obtained in the percolation case.

Fig. 8 shows averaged plots $\ln P$ versus $\ln \overline{S_2}$ for the case of Th for several values of Z_1Z_2 at which the cuts are made. In this figure each averaged plot is obtained by excluding all fission events that have a value of Z_1Z_2 greater than or equal to the indicated value and then averaging over all the remaining events having the same value of $\ln P$ to get the value of $\overline{S_2}$. Apart from the subtraction of the fission events, this averaging process is the same as that used in the percolation case to produce fig. 2. It is seen that if the fission events are not removed the resulting averaged plot is very different from that for a percolation problem with a comparable lattice size (see fig. 2). Moreover a cut at $Z_1Z_2 = 700$ produces the smoothest curve with a well-rounded critical region. A cut at lower values of Z_1Z_2 produces a sharp corner at the meeting point of the two branches while a cut at higher values of Z_1Z_2 produces an elongated corner which differs from that obtained in pecolation. Moreover, by examining fig. 6, it is seen that the cut at $Z_1Z_2 = 700$ corresponds to a naturally occurring, though not so deep, valley. The values of 500 and 900 used

for the cuts in fig. 8 correspond approximately to the lower and upper borders of the "valley" that separates the hot fission peak from the remaining events in fig. 7.

Fig. 9 shows plots of ln P versus the logarithm of the corresponding average second moment of the charge distribution ln $\overline{S_2}$ for six different nuclear systems: ^{131}Xe, ^{165}Ho, ^{197}Au, ^{209}Bi, ^{232}Th and ^{252}Es. In each case the hot fission events are removed by excluding all events with $Z_1Z_2 \geq$ "an optimal value" obtained in the manner described above for ^{232}Th. The optimal values of Z_1Z_2 for the systems considered here are found, in ascending order of the mass of the system, to be 400, 500, 550, 600, 700 and 750. For the small systems, ^{131}Xe and ^{165}Ho, very few fission events are produced or removed. These plots for the nuclear case are to be compared with the similar plots in fig. 2 for the percolation case which, it must be remembered, covers a larger range of system sizes.

The slopes of the lower branches of the plots in fig. 9 are found by a least-squares-fit to be, in the same order as above, 2.410 ± 0.088, 2.504 ± 0.111, 2.626 ± 0.067, 2.562 ± 0.068, 2.573 ± 0.074 and 2.281 ± 0.092. These values are much larger than the theoretically expected value $1 + \beta/\gamma = 1.265$ for a liquid-gas phase transition as well as the values obtained in percolation. This difference is, at least, partially, a reflection of the fact that the sizes (i.e. charges) of the nuclear systems investigated are very small, $54 \leq Z \leq 99$, whereas the value .265 is expected to hold for very large systems. However, the slopes obtained for percolation systems of comparable size do not show such large deviations. For example from the percolation results of the previous section for $L = 4$ and $L = 5$, which have 64 and 125 sites, respectively, we got slopes

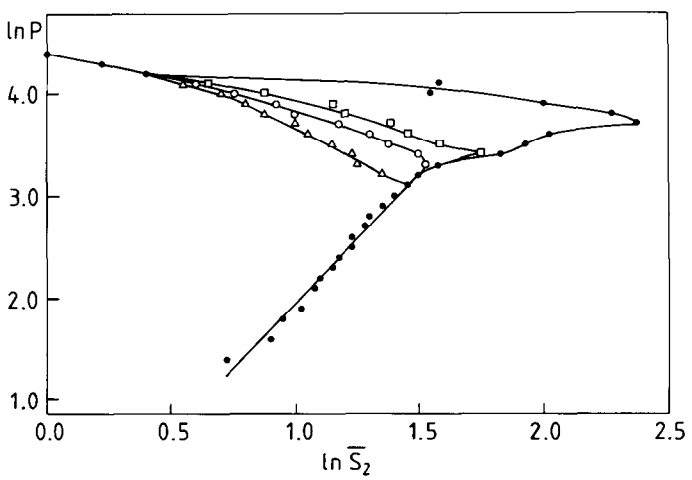

Fig. 8. Plots of the logarithm of the largest fragment charge $P(=Z_1)$ produced versus the logarithm of the corresponding average second moment $\overline{S_2}$ for the microcanonical multifragmentation of hot ^{232}Th nuclei. The various plots correspond to different values of Z_1Z_2 used to subtract the fission events. The triangles, open circles and squares correspond to excluding fission events with $Z_1Z_2 \geq 500$, 700 and 900, respectively. The dots correspond to the case where the fission events are not excluded from the averaging. The continuous curves are just to guide the eye.

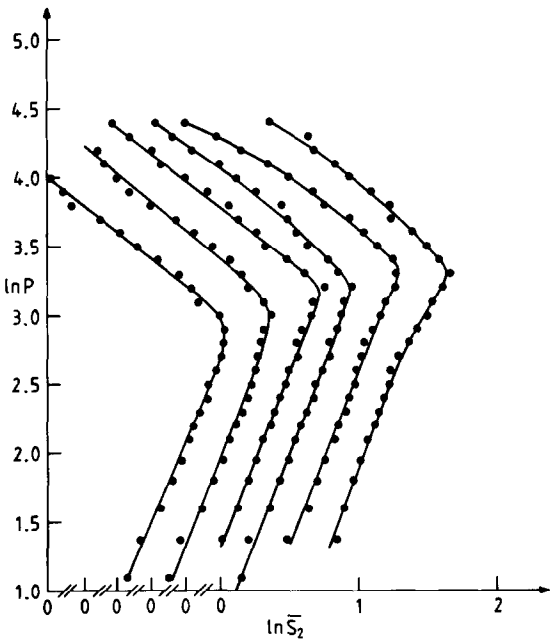

Fig. 9. The logarithm of the largest fragment size P as a function of the logarithm of the corresponding average second moment $\bar{S}_2$ for 6 different nuclear systems: ^{131}Xe, ^{165}Ho, ^{197}Au, ^{209}Bi, ^{232}Th and ^{252}Es arranged from left to right in ascending order of the mass of the system. The dots represent the actual calculation results and the curves drawn are just to guide the eye. Note that the $\ln \bar{S}_2$ scale given corresponds to the heaviest system ^{252}Es. The other curves are successively shifted to the left with respect to each other by a distance of 0.25.

of 1.582 ± 0.036 and 1.503 ± 0.029. This indicates that the small size by itself cannot be responsible for such a discrepancy.

One possible reason for this discrepancy is that the *Coulomb force modifies the liquid-gas transition itself* and that its role is not simply limited to the production of the subtracted hot fission events. However, there are sources of error that can also contribute to the discrepancy. One such source of error that can affect the value of the slope is the way the fission events are removed. Another source of uncertainty is whether the slope is to be determined from the few points close to the critical point or from the whole lower branch as has been done here so far. In the percolation case we have excluded the events far removed from the critical region. In this respect, it is interesting to note that near the middle of the lower branch for the two largest systems there is a change of slope with the two part of the branch being less steep. In fact, if we only consider the top 8 points of the lower branch for the heaviest system ^{252}Es the best fit yields a slope of 1.611 ± 0.034 which is consistent with the values quoted above for the smallest percolation systems.

In contrast to the slope of the lower branch, the determination of the largest fragment at the critical point P_c depends on the subtraction of the hot fission events.

Whereas in the percolation case it was found adequate to infer the size of P_c from the plots in fig. 2 by merely reading-off the value of P with the largest value of $\overline{S_2}$, more care was necessary in applying the same procedure for the nuclear case as the value of P_c was found to be quite sensitive to the value of Z_1Z_2 at which the subtraction of the fission events is carried out. In order to reduce this sensitivity the 7 "data" points closest to the meeting point of the upper and lower branches were fit by a polynomial of degree 3 and the location of P_c was determined from this fit. This procedure was found to reduce the above-mentioned sensitivity to within the uncertainty inherent in using finite-size bins for the values of $\ln P$. Comparable results were also obtained with a polynomial of degree 2 (i.e. parabola). The inclusion of more points in obtaining the fit would lead to an error in determining P_c due to the influence on the fit by points far removed from the critical region.

In fig. 10 we show a log-log plot of the values of P_c obtained in the manner described in the previous paragraph as a function of the linear size of the corresponding nuclear system $L = Z^{1/3}$ where Z is the total charge of that system. The error bars in this figure reflect the size of the bins of $\ln P$ or the uncertainty due to the subtraction of the fission events, whichever is larger. The slope of the straight line fitting these points should equal the fractal dimension (see eq. (6)). A least-squares fit yields $D = 2.36 \pm 0.15$ which is to be compared with $D = 2.480$ in table 1.

The determination of the slope of the upper branch is of course very sensitive to the subtraction of the fission events. The slopes corresponding to the optimal value of Z_1Z_2 are always larger in magnitude than the theoretically expected value $-\beta/\gamma = -0.265$. For example, the slope of the least-square straight-line fit to the upper branch of the heaviest system in fig. 9 is found to be -0.873 ± 0.036. Again

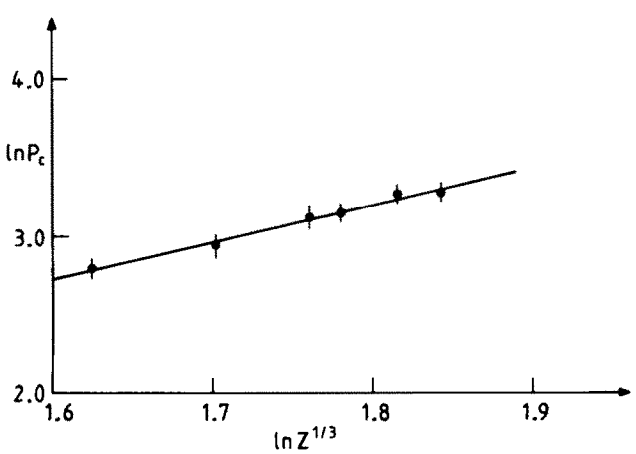

Fig. 10. The logarithm of the largest fragment size at the critical point P_c as a function of the logarithm of the corresponding linear size of the system $L = Z^{1/3}$ for the microcanonical multifragmentation of the various nulear systems of the previous figure.

this discrepancy may reflect the very small size of the systems considered as well as a possible modification of the properties of the phase transition by the Coulomb force.

A finite-size-scaling analysis of the curves for the 6 nuclear systems according to the ansatz given in eq. (14) is shown in fig. 11. The optimal value of θ is found to be 1.35 which is to be compared with the theoretically expected value $\theta = 1.96$ (see eq. (15) and table 1). The difference, as in the case of percolation may be attributable to higher-order corrections to finite-size scaling. These corrections are more important here than in the percolation cases because of the much smaller sizes of the nuclear systems. This limitation on the nuclear system sizes is of course dictated by the peculiarity of the nuclear problem and not by any computational or other limitations. In trying to find the optimal value of D it is seen from fig. 11 that there is a range of values that produce equally acceptable results. The case with $D = 2.10$ may be seen to produce the best result but the case with $D = 2.55$ is also acceptable. Both of these values are comparable to the value obtained from fig. 10. However, even the case with $D = 3$ cannot be rejected off-hand. As a matter of fact, a close inspection of the critical region reveals that $D = 3$ provides better scaling for 4 of the systems. One of the remaining systems (^{252}Es) is inadequately described in the three cases. This ambiguity in the value of D is due to the small range of nuclear sizes available, in contrast to the percolation case where the sizes considered ranged

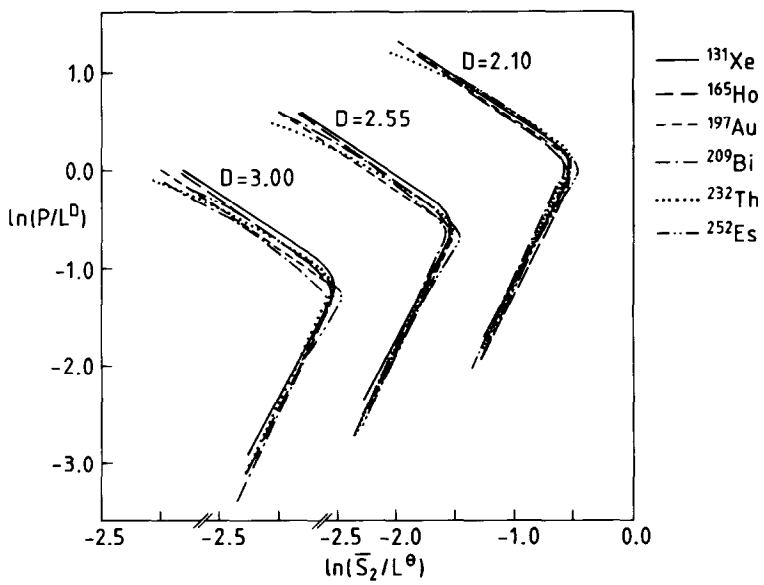

Fig. 11. Finite-size-scaling analysis of the $\ln P$ versus $\ln \overline{S_2}$ plots for the various nuclear systems investigated. For clarity, we do not show the dots representing the actual results of the calculation, but we show smooth curves drawn through these dots similar to the curves drawn in fig. 9. Each of the three sets of curves corresponds to a different value of D as indicated, but they all have the same value of $\theta = 1.35$.

from 64 to 1000 which enabled us to easily distinguish between the various values of D.

The physical meaning of a value of D less than the euclidean dimension d in the nuclear case must be examined carefully. It is tempting to interpret $D < d$ [ref. [38])] as reflecting the existence of "pre-fragments" that contain many holes inside them and that later deexcite to become the detected normal compact fragments. However, it must be pointed out that in our microcanonical nuclear fragmentation calculation we start from an equilibrium situation consisting of "normal compact" fragments which have a mass that scales as R^3 and no reference is made to any "pre-fragments" or to the way these fragments are formed. The occurrence of a value of $D < d$ may however be another indication of the lingering role of the long-range Coulomb force. In addition to being responsible for the hot fission-events, the Coulomb force may also modify the properties of the two main branches corresponding to the nuclear liquid-gas transition.

5. Conclusion

In conclusion we have analyzed the cluster size distributions obtained for systems of various sizes in percolation and in nuclear fragmentation. We first applied the methods used to the percolation systems where the properties of the relevant phase transition are well understood and verified that the methods employed are dependable. These methods essentially depend on finding the correlation between the largest cluster or fragment P in each event and the corresponding second moment S_2 of the remaining clusters. Average plots derived from this correlation were then used, together with finite-size scaling, to derive values for the fractal dimension D and the ratios of the critical exponents β/γ and γ/ν. In the case of percolation the systems considered ranged in size from $4^3 = 64$ to $10^3 = 1000$ sites and the results obtained were in good agreement with the asymptotic values currently available in the literature.

In the nuclear case the analysis suffered from two main difficulties. The first difficulty concerns the problem of the removal of the hot fission events. This problem is very interesting in light of the fact that very little is known, whether experimentally or theoretically, about the fissility of hot nuclei. The second difficulty arises out of the fact that the range of nuclear systems available is very limited so that the calculations in this case were limited to systems with total charge in the range $54 \leq Z \leq 99$ which is much narrower than the range covered in percolation. Both of these difficulties lead to large uncertainties and ambiguities in interpreting the results.

The plots resulting from the nuclear events, with the hot fission events subtracted, tended to have a qualitative similarity with the plots obtained in percolation. This similarity indicates that in both cases a phase transition takes place. However, the quantitative uncertainties in the results in the nuclear case prevented us from definitely identifying the nature of this transition which we believe to be related to

the liquid-gas phase transition in nuclear matter. There are indications however that the effect of the Coulomb force may not be limited to the production of hot fission fragments and that it actually modifies the properties of the liquid-gas phase transition so that the procedure of simply excluding the hot fission events followed here may not be sufficient. This may be partly responsible for the fact that the slopes and critical exponents evaluated for the nuclear case deviate significantly from their expected values and from the values for percolation systems of comparable size. This interesting and important problem of finite many-body systems deserves more theoretical investigation. The associated phenomenon of hot nuclear fission should also be worthy of further theoretical and experimental study.

Finally, it must be emphasized that the presented calculations of statistical nuclear fragmentation are carried out within a model that has its limitations. Some of these limitations like the assumption of equilibrium multifragmentation are inherent in the model, while others reflect certain approximate treatments that can eventually be improved. One such approximation that may be important and that is in the process of being improved is the treatment of secondary or delayed evaporation of charged particles. In the present work, such evaporation is only included in a rough way [25]). However, it is not expected that this will appreciably change the present results which we hope will provoke better experiments to probe this very interesting and far-reaching problem. Such experiments must be sufficiently exclusive to allow the determination of the second moment of the fragment size or charge distribution. There is no need to measure the momenta or energies of these fragments.

In a pioneering work Campi [38]) was the first to try a sealing analysis of about 400 events from ref. [36]).

One of the authors (H.R.J) would like to thank the Alexander von Humboldt Foundation for financial support and the Hahn-Meitner-Institut for its hospitality.

References

1) M.W. Curtain, H. Toki and D.K. Scott, Phys. Lett. **B123** (1983) 289;
A.D. Panagiotou, M.W. Curtain, H. Toki, D.K. Scott and P.J. Siemens, Phys. Rev. Lett. **52** (1984) 496
2) G. Bertsch and Philip J. Siemens, Phys. Lett. **B126** (1983) 9
3) A.L. Goodman, J.I. Kapusta and A.Z. Mekjian, Phys. Rev. **C30** (1984) 851
4) H.R. Jaqaman, Gabor Papp and D.H.E. Gross, Nucl. Phys. **A514** (1990) 327
5) R.G. Palmer and P.W. Anderson, Phys. Rev. **D9** (1974) 3281
6) W.G. Kupper, G. Wegmann and E.R. Hilf, Ann. of Phys. **88** (1974) 454
7) G. Sauer, H. Chandra and U. Mosel, Nucl. Phys. **A264** (1976) 221
8) P. Danielewicz, Nucl. Phys. **A314** (1979) 465
9) D.Q. Lamb, J.M. Lattimer, C.J. Pethick and D.G. Ravenhall, Phys. Rev. Lett. **41** (1978) 1623; Nucl. Phys. **A360** (1981) 459
10) H. Schulz, L. Münchow, G. Röpke and M. Schmidt, Phys. Lett. **B119** (1982) 12; Nucl. Phys. **A399** (1983) 587
11) H.R. Jaqaman, A.Z. Mekjian and L. Zamick, Phys. Rev. **C27** (1983) 2782

12) J.E. Finn, S. Agarwal, A. Bujak, J. Chuang, L. Gutay, A.S. Hirsch, R.W. Minich, N.T. Porile, R.P. Scharenberg, B.C. Stringfellow and F. Turkot, Phys. Rev. Lett. **49** (1982) 1321; Phys. Lett. **B118** (1982) 458
13) H.H. Gutbrod, A.I. Warwick and H. Wieman, Nucl. Phys. **A387** (1982) 177c
14) D.H.E. Gross, L. Satpathy, Meng Ta-chung and M. Satpathy, Z. Phys. **A309** (1982) 41
15) H.R. Jaqaman, A.Z. Mekjian and L. Zamick, Phys. Rev. **C29** (1984) 2067
16) S. Levit and P. Bonche, Nucl. Phys. **A437** (1985) 426
17) H.R. Jaqaman, Phys. Rev. **C39** (1989) 169; **C40** (1989) 1677
18) A.R. DeAngelis and A.Z. Mekjian, Phys. Rev. **C40** (1989) 105
19) C. Domb, Proc. Phys. Soc. **86** (1965) 933;
M.E. Fisher and A.E. Ferdinand, Phys. Rev. Lett. **19** (1967) 169;
A.E. Ferdinand and M.E. Fisher, Phys. Rev. **185** (1969) 832;
M.E. Fisher in, Critical Phenomena, Proc. Int. School of Physics "Enrico Fermi", course 51, ed. M.S. Green (Academic Press, New York, 1971)
20) X. Campi, J. of Phys. **A19** (1986) L917
21) X. Campi, Phys. Lett. **B208** (1988) 351; and J. de Phys. **50** (1989) 183
22) K. Binder in, Phase transitions and critial phenomena, ed. C. Domb and M.S. Green, vol. 5B (Academic Press, New York, 1976).
23) M.N. Barber, in Phase transitions and critical phenomena, ed. C. Domb and J.L. Lebowitz, vol. 8 (Academic Press, New York, 1983)
24) D.H.E. Gross and B.H. Sa, Nucl. Phys. **A437** (1985) 643;
X.-Z. Zhang, D.H.E. Gross, S.-Y. Xu and Y.-M. Zheng, Nucl. Phys. **A461** (1987) 641; 668
25) D.H.E. Gross, Rep. Prog. Phys. **53** (1990) 605
26) D. Stauffer, Introduction to percolation theory, (Taylor and Francis, London, 1985); Phys. Reports **54** (1979) 1
27) G. Grimmett, Percolation (Springer, New York, 1989)
28) H.E. Stanley, Introduction to phase transitions and critical phenomena, (Clarendon, Oxford, 1971)
29) M.E. Fisher, Phys (N.Y.) **3** (1967) 255
30) D. Staufer, in Growth and form, ed. H.E. Stanley and N. Ostrowsky (Nijhoff, Dordrecht, 1986);
P. Grassberger, J. of Phys. **A19** (1986) 1681
31) M.E. Fisher, Proceedings on Critical phenomena, Stellenbosch, South Africa 1982, ed. F.J.W. Hahne (Springer, Berlin, 1983)
32) N. Jan, D.L. Hunter and T. Lookman, Phys. Rev. **B29** (1984) 6356
33) J. Randrup and S.E. Koonin, Nucl. Phys. **A356** (1981) 223;
S.E. Koonin and J. Randrup, Nucl. Phys. **A474** (1987) 173;
G. Fai and J. Randrup, Nucl. Phys. **A487** (1988) 397
34) J.P. Bondorf, R. Donangelo, I.N. Mishustin and H. Schulz, Nucl. Phys. **A444** (1985) 460;
H.W. Barz, J.P. Bondorf, R. Donangelo, I.N. Mishustin and H. Schulz, Nucl. Phys. **A448** (1986) 753
35) A.Y. Abul-Magd, W.A. Friedman and J. Hüfner, Phys. Rev. **C34** (1986) 113
36) C.J. Waddington and P.S. Friar, Phys. Rev. **C31** (1985) 888
37) X. Campi, private communication
38) X. Campi, Nucl. Phys. **A495** (1989) 259c